Scientific research article / https://doi.org/10.15446/rcciquifa.v52n2.110734

Bone therapy through drug delivery of chelated [bisphosphonate-metal ions] adsorbed on the surface of carbon nanotubes

Fatemeh Mollaamin[1*], Majid Monajjemi[2]

[1]Department of Food Engineering, Faculty of Engineering and Architecture, Kastamonu University, Kastamonu, Turkey.

[2]Department of Chemical Engineering, Central Tehran Branch, Islamic Azad University, Tehran, Iran.

*Corresponding author e-mail: smollaamin@gmail.com

Received: August 6, 2022
Corrected: March 15, 2023
Accepted: March 22, 2023

Summary

Aim: To investigate asingle-walled carbon nanotube (SWCNT) joint to bisphosphonate agents of 5AEL, 5AFX, 4QPF, 3DYG, 2F92, 2I19 chelated to metal cations of Mg^{2+}, Ca^{2+}, Sr^{2+} due to the direct electron transfer principle which has been studied by density functional theory methods. **Method:** It has been accomplished the B3LYP/6-311+G(d,p)/LANL2DZ to estimate the susceptibility of SWCNT for adsorbing 5AEL, 5AFX, 4QPF, 3DYG, 2F92, 2I19 chelated to metal cations of Mg^{2+}, Ca^{2+}, Sr^{2+} through nuclear magnetic resonance and thermodynamic parameters. **Results:** The data explained that the feasibility of using SWCNT and bisphosphonate agents becomes the norm in metal chelating of delivery system, which has been selected through several bisphosphonate agents of 5AEL, 5AFX, 4QPF, 3DYG, 2F92, and 2I19 using DFT method due to physico-chemical properties of NMR and IR methodologies.

Keywords: (5,5) armchair SWCNT, protein-bisphosphonate, metal chelating.

Resumen

Terapia ósea a través de la administración de fármacos tipo quelatos [iones bisfosfonato-metal] adsorbidos en la superficie de nanotubos de carbono

Objetivo: investigar la unión de nanotubos de carbono de pared simple (SWCNT) con agentes bisfosfonatos de 5AEL, 5AFX, 4QPF, 3DYG, 2F92, 2I19 quelados con cationes metálicos de Mg^{2+}, Ca^{2+}, Sr^{2+} debido al principio de transferencia directa de electrones que tiene ha sido estudiado por métodos de la teoría funcional de la densidad. **Método:** se ha realizado el B3LYP/6-311+G(d,p)/LANL2DZ para estimar la susceptibilidad de SWCNT para adsorber 5AEL, 5AFX, 4QPF, 3DYG, 2F92, 2I19 quelados a cationes metálicos de Mg^{2+}, Ca^{2+}, Sr^{2+} mediante resonancia magnética nuclear y parámetros termodinámicos. **Resultados:** los datos explicaron que la viabilidad de usar SWCNT y agentes bisfosfonatos se convierte en la norma en el sistema de entrega de quelación de metales, que ha sido seleccionado a través de varios agentes bisfosfonatos de 5AEL, 5AFX, 4QPF, 3DYG, 2F92 y 2I19 usando el método DFT debido a propiedades fisicoquímicas de los métodos de RMN e IR.

Palabras clave: (5.5) sillón SWCNT, proteína-bifosfonato, quelación de metales.

Resumo

Terapia óssea por meio de administração do quelatos [íons bifosfonato-metal] adsorvidos na superfície de nanotubos de carbono

Objetivo: investigar os nanotubos de carbono de parede simples (SWCNT) unidos a agentes bifosfonatos de 5AEL, 5AFX, 4QPF, 3DYG, 2F92, 2I19 quelatados a cátions metálicos de Mg^{2+}, Ca^{2+}, Sr^{2+} devido ao princípio de transferência direta de elétrons que tem tem sido estudado por métodos da teoria do funcional da densidade. **Metodo:** foi realizado o B3LYP/6-311+G(d,p)/LANL2DZ para estimar a suscetibilidade do SWCNT para adsorver 5AEL, 5AFX, 4QPF, 3DYG, 2F92, 2I19 quelatados a cátions metálicos de Mg^{2+}, Ca^{2+}, Sr^{2+} por ressonância magnética nuclear e parâmetros termodinâmicos. **Resultados:** os dados explicaram que a viabilidade do uso de agentes SWCNT e bisfosfonatos se torna a norma no sistema de entrega de quelante de metal, que foi selecionado por meio de vários agentes bisfosfonatos de

5AEL, 5AFX, 4QPF, 3DYG, 2F92 e 2I19 usando o método DFT devido a propriedades físico-químicas de metodologias de RMN e IV.

Palavras-chave: (5,5) poltrona SWCNT, proteína-bifosfonato, quelantes de metais.

Introduction

Bone tissue tolerates constant rebuilding and achieves the equilibrium by osteoblasts producing bone and osteoclasts destroying bone. The compounds of bisphosphonates keep from the digestion of bone by pushing osteoclasts to bear cell death or the apoptosis, which diminish the velocity of bone destroying [1].

The principal impact of the active bisphosphonates is to prevent bone resorption. In fact, these structures manifest to be strong inhibitors of resorption when experimented in various conditions of in vivo and in vitro. Bisphosphonate compounds stop bone resorption produced by different reasons in cell and organ. They prevent forming the holes by isolated osteoclasts on mineral layers [2].

Generally, the physicochemical impacts of bisphosphonates are very close to those of pyrophosphate. Therefore, they prevent the formation, postpone the association, and decrease the dissolution of calcium phosphate compounds. All these impacts depend on the identified intention of these structures for solid-phase calcium phosphate, on the surface of which they attach extremely. This notable characteristic is the basis for the employment of these structures as skeletal markers in nuclear medicine and the foundation for their selective localization in bone when employed as the drugs. There is an attention to enhancing the bioavailability and duration of action of a drug to modify therapeutic consequences. Drug delivery technique is able to change a drug's pharmacokinetics and specificity by formulating it with various ingredients, drug carriers, and medical equipment [3-7].

Nanomedicine covers a wide range of therapeutic applications, from nanoparticulate drug delivery systems including carbon nanotubes, layered double hydroxides, to in vitro (biosensor) and in vivo (imaging and implantable devices) diagnostics [8-13]. Nanomedicine in drug delivery is for achieving the improved delivery of water insoluble drugs, delivery of large macromolecule drugs to intracellular sites of action, and codelivery of two or more drugs or therapeutic agents for combination remedy [14-16]. Since the exploring CNTs in 1990s and the progress of their application in nanomedicine, these compounds are significant through their properties including rich electronic and thermal factors, great mechanical strength, high chemical stability, and

extremely lightweight [17-19]. These carriers indicate the capability for transferring the therapeutic agents such as proteins, DNA, antibodies and drugs on the external wall or by trapping in the cavity nanotubes as a capsule [20-22].

Nanotubes with their intrinsic properties have been considered potential candidates for drug delivery carriers. The capped ends of nanotubes may be opened up by oxidation, allowing for the insertion of molecules of interest inside the nanotube. Carbon nanotubes (CNTs) can easily penetrate cells, delivering drugs directly to the cytoplasm or nucleus.

CNTs are large molecules that are built by repeating pattern of sp^2 hybridized carbon atoms in a hexagonal composition, rolled into a cylinder of approximately 2.5-100 nm in diameter. CNTs are long and tubular fullerene structures, which can be either single-walled (SWCNTs) or multiwalled (MWCNTs). SWCNTs are formed by a rolling single layer of graphite cylinder with a tube diameter of approximately 0.4-2 nm, but MWCNTs are multiple concentric cylindrical shells of graphite layers with the distance about 0.36 nm and diameters about 2-100 nm. Nanotubes conform to a perpendicular position with the cell membrane during uptake, perforating and diffusing through the lipid bilayer to enter the cytoplasm. Functionalized CNTs are easily internalized by cells through passive and endocytosis-independent mechanisms [1-6].

The bone cells in human body are gradually being continually taken away and substituted with new ones by osteoblast in the total life. The bisphosphonates behave by reducing osteoclast activity and then reducing the overturn of bone or replacement of the old bone cell. Since we start being old and in particular, a disease, the bone is really being damaged or removed more quick than our body can substitute it. This makes the bones weakened, thin and much easily to break with even a small impact or a fall from a standing height. Therefore, bisphosphonate medications support us to keep the bone density and bone strength.

In fact, the most popular bisphosphonate medications have a rich tension for metal cations, among them Ca^{2+}, with which they can produce both soluble and insoluble compounds and aggregates, depending on the pH of the solution and the metal exist. The bisphosphonates are separated into chemical branches based on the side chains of R1 and R2. It is seen a central carbon in bisphosphonates with two side chains of R1, R2 and two phosphate branches which are bonded to Ca^{2+} through O- of PO_3 groups for keeping a high amount of Ca^{2+} in bones of human body cells (Scheme1) [23-29].

In this article, we have focused more on recent bisphosphonate drugs such as 5AEL, 5AFX,4QPF, 3DYG, 2F92, 2I19 which have been chelated with Mg^{2+}, Ca^{2+}, Sr^{2+} adsorbed onto (5,5) armchair SWCNT, respectively (Scheme1). This new generation of

bisphosphonates agents of 5AEL, 5AFX, 4QPF, 3DYG, 2F92, 2I19 as second and third generation of bisphosphonates consist of nitrogen atoms in side chain of R2 for promoting osteoclast apoptosis (Scheme1).Therefore, sicks obtain the cure with more intense nitrogen bisphosphonates rather than the earlier non nitrogen bisphosphonates.

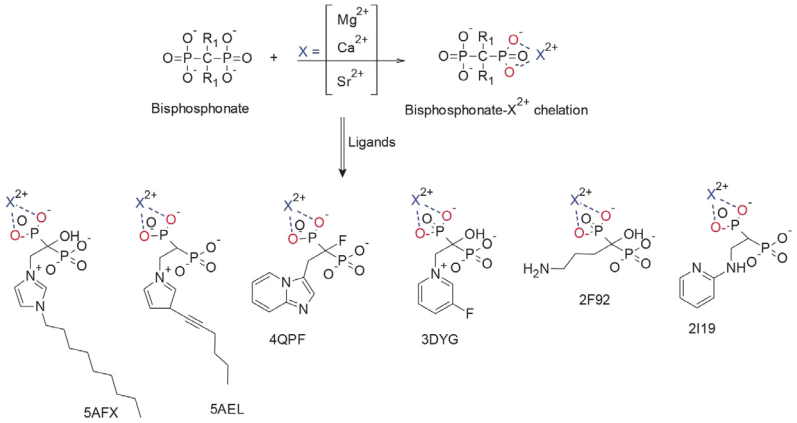

Scheme 1. Proposed mechanism of bisphosphonate- metal cation chelation of $Mg^{2+}/Ca^{2+}/Sr^{2+}$ through the O^- of two PO_3 (phosphonate) groups covalently linked to carbon for six ligands of 5AEL,5AFX,4QPF,3DYG,2F92 and 2I19.

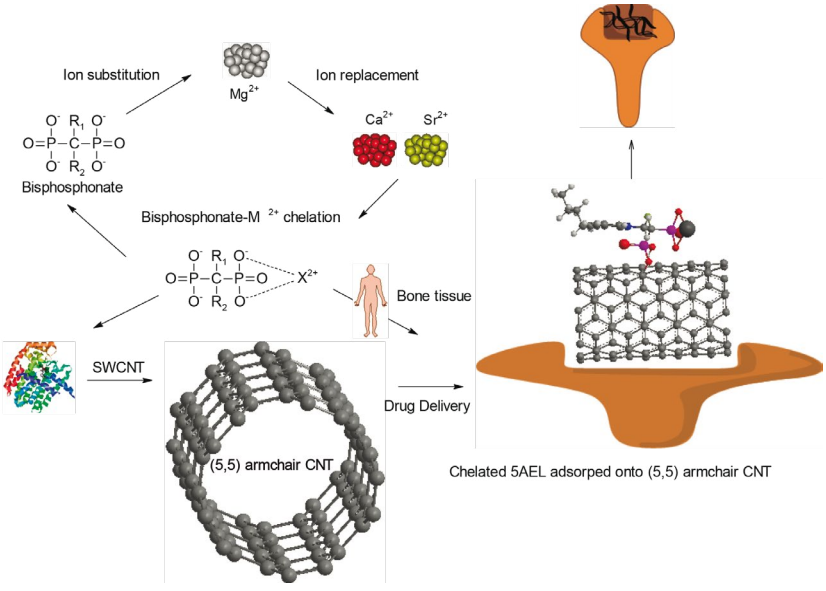

Scheme 2. Drug delivery of (5,5) armchair-SWCNT jointed with bisphosphonate agents of 5AEL, 5AFX,4QPF, 3DYG, 2F92, 2I19 chelated with Mg2+, Ca2+, Sr2+ in the bone of human body.

The chelation of bisphosphonate agents of 5AEL, 5AFX,4QPF, 3DYG, 2F92, 2I19 with Mg^{2+}, Ca^{2+}, Sr^{2+} has been investigated in this study by forming relatively stable drugs for adsorption onto (5,5) armchair CNT as a drug deliver (Scheme2). Thus, a series of quantum theoretical approaches has been accomplished for finding the optimized coordination of [bisphosphonate- Mg^{2+}, Ca^{2+}, Sr^{2+} - (5,5) armchair CNT] chelation with DFT method of computations using Gaussian09 program package (Figure1) [30].

(a)

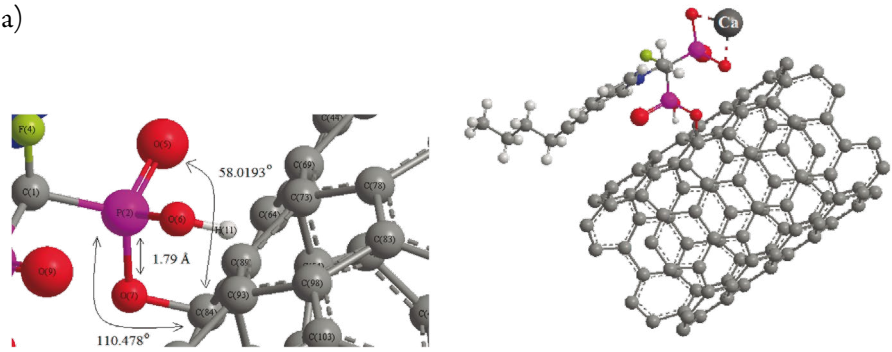

(b)

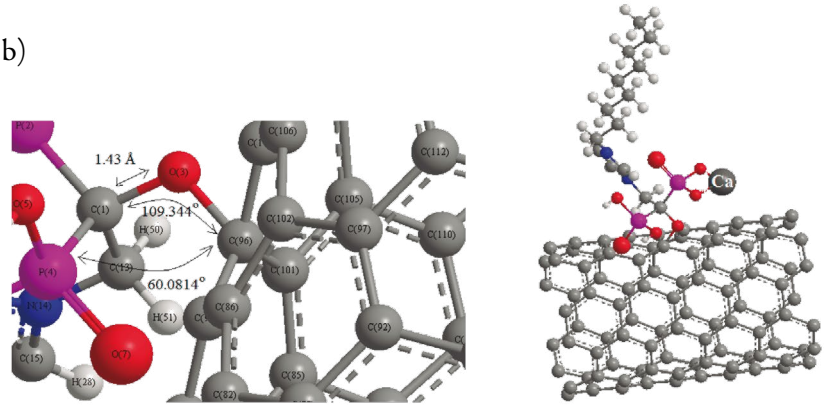

(c)

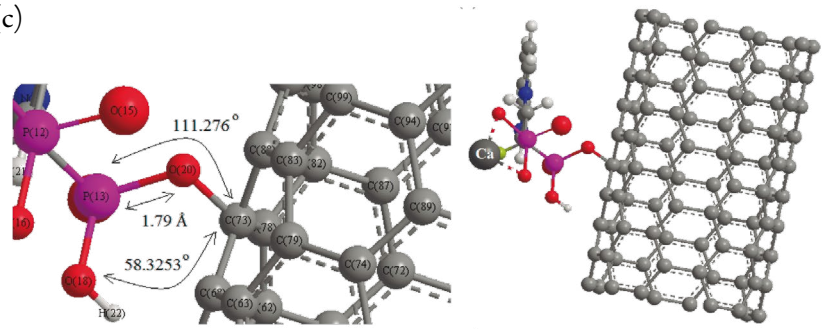

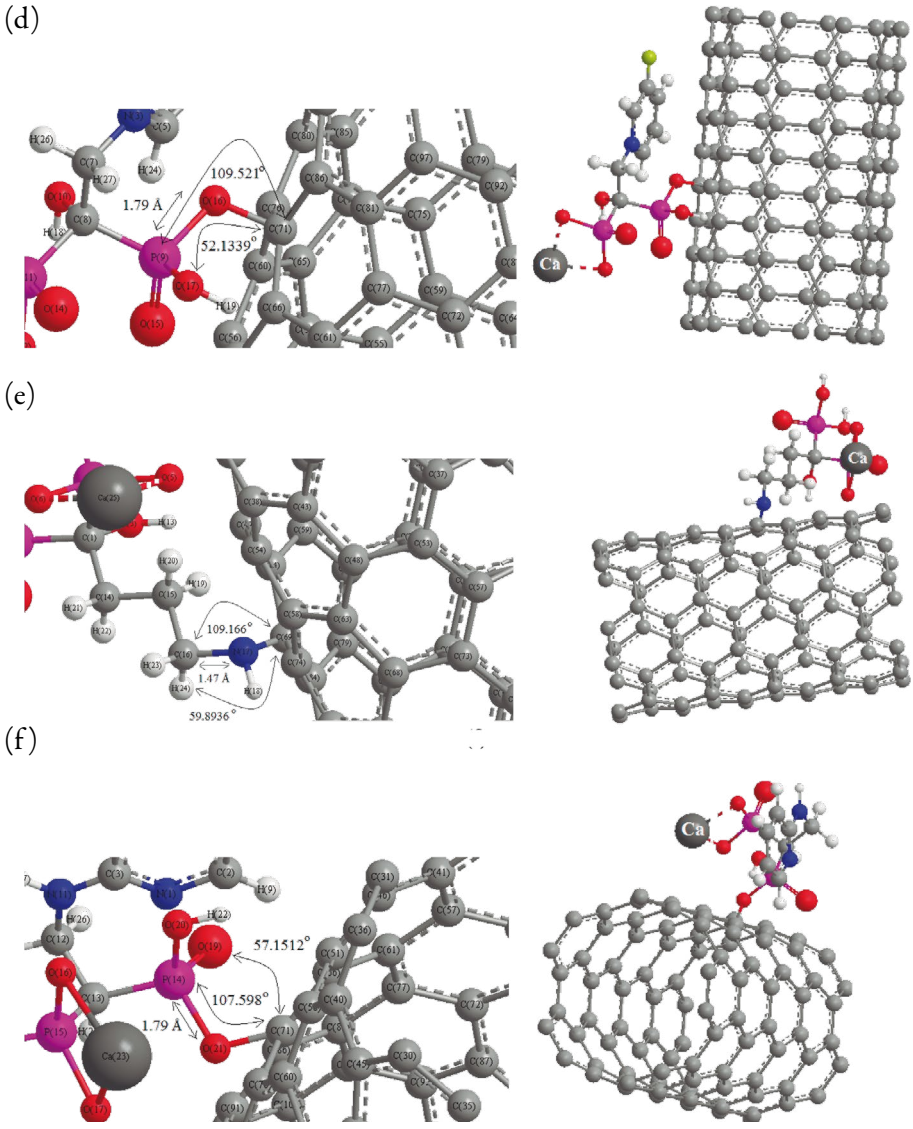

Figure 1. Adsorption of a) 5AEL, b) 5AFX, c) 4QPF, d) 3DYG, e) 2F92, f) 2I19 chelated with Ca^{2+} onto surface of (5,5) armchair CNT.

Theoretical background and computational method

The density functional theory (DFT) is one of the most employed approximations of Hohenberg, Kohn and Sham, which permit the theoretical study of material properties [31]. DFT theory proves an advantageous method for predicting chemical systems, and in order to understand its similarities and differences to other computational methods employed.

In this study, the geometries were optimized at the framework of DFT using the three-parameter Becke's exchange [32, 33] and Lee-Yang-Parr's correlation non-local functional [34, 35], usually known as B3LYP method and basis sets of lnl2dz for metal cations of Mg^{2+}, Ca^{2+}, Sr^{2+} and 6-311+G(2d,p) for other atoms including H,C,N,O,F,P. Then, it has been described the electronic structure of adsorbed (5,5) armchair SWCNT by bisphosphonate agents of 5AEL, 5AFX,4QPF, 3DYG, 2F92, 2I19 chelated with Mg^{2+} ,Ca^{2+}, Sr^{2+} for measuring physico-chemical properties (Figure 1).

In this investigation, the Onsager model has been accomplished that was developed by Frisch, Wong and Wiberg utilizes spherical cavities. Even though this implies a less accurate description of the solute-solvent interface, this approximation simplifies the evaluation of energy formatives in geometry optimizations, and frequency analysis. Moreover, Cramer and Truhlar improved this model at dipole level [36-40]. In fact, a cavity must have a physical sense such as Onsager model, and has a mathematical ability as often happened in other descriptions of solvent impacts [41]. Specially, the cavity has to keep out the solvent and including its frontiers as the biggest probability part of the solute charge distribution [41].

Then, The gauge including atomic orbitals (GIAO) has been adopted to solve the gauge problem in the calculation of nuclear magnetic shielding for the complexes of 5AEL, 5AFX,4QPF, 3DYG, 2F92, 2I19 chelated with Mg^{2+}, Ca^{2+}, Sr^{2+} adsorbed onto (5,5) armchair SWCNT using density functional theory (DFT) calculations.

These new drugs have been used for new lower bone tendency of bisphosphonate drug design which is sufficient curing diseases identifying by abnormal bone resorption (4QPF). The progress of selective protein farnesyl transferase (FTase) and protein geranylgeranyl transferase (GGTase) inhibitors as anticancer therapeutic agents has explored 3DYG which is more efficient than current bisphosphonate drugs [42]. 2I19 is a solid-state (13)C, (15)N, and (31)P magic-angle sample spinning (MAS) NMR and quantum chemical study of several bisphosphonates as pure structures and bonded

to FPPS for preparing data collection about side chain and phosphonate backbone protonation states when bind to the enzyme [43]. It has been indicated the consequences of many potential prenyl synthase inhibitors against Trypanosoma brucei farnesyl diphosphate synthase (TbFPPS) and against T. brucei, the causative agent of human African trypanosomiasis. 5AFX is one of the most powerful compounds lipophilic analogs of the bone resorption medication of zoledronate family [44]. 2F92 has been attained by solving the crystal structures of human farnesyl pyrophosphate synthase (FPPS) in its unliganded state, in complex with the nitrogen containing bisphosphonate (N-BP) medications of , alendronate , ibandronate, pamidronate, zoledronate which prepare a new achieving of the mechanism of FPPS catalysis and inhibition [45].

A type of linkage of molecules to metal ions is chelation which defines the presence of two or more coordinated bonds between a multiple bonded ligand that are known chelating or sequestering agents and a single central metal atom. Chelation can be used between drugs and metal ions. For example, antibiotic drugs of the tetracycline and quinolone families are chelating agents of Fe^{2+}, Ca^{2+}, and Mg^{2+} ions [46, 47].

The chelation of bisphosphonates with cations in bone cells has been accomplished in this research by forming relatively stable complexes. Therefore, a group of quantum theoretical methods has been run for exploring the optimized structures of [bisphosphonatecations of Mg^{2+}/ Ca^{2+}/Sr^{2+}] cluster chelation adsorbed onto the surface of (5,5) armchair SWCNT as the drug delivery method in human bone with thermodynamic calculations and nuclear magnetic resonance analysis using Gaussian 09 program software [30, 48].

Results and discussion

CNTs are representing drug delivery platforms that can be functionalized with various biomolecules including antibodies, proteins, and DNA. This permits the particular targeted for transferring the special tissues, organs, or cells. These compounds can easily penetrate cells, delivering drugs directly to the cytoplasm or nucleus. Drug delivery systems improve the pharmacological and therapeutic profile and efficacy of the drug and lower the occurrence of off-targets.

NMR analysis

The NMR data of isotropic (σ_{iso}), anisotropic shielding tensor (σ_{aniso}), and eigenvalues of chemical shielding including σ_{11}, σ_{22}, σ_{33} for 5AEL, 5AFX, 4QPF, 3DYG, 2F92, 2I19 adsorbed onto (5,5) armchair SWCNT, respectively, have been estimated (Table 1).

Table 1. SCF GIAO Magnetic shielding tensor for 5AEL, 5AFX, 4QPF, 3DYG, 2F92, 2I19 in ppm chelated with cations at the adsorption site onto (5,5) armchair SWCNT.

5AEL										
ppm	**P2**	**P3**	**F4**	**O5**	**O6**	**O7**	**O8**	**O9**	**O10**	**N12**
σ_{11}	120.7202	230.1554	435.8378	-845.9768	294.3757	235.7504	288.5618	-865.3928	282.1969	248.4936
σ_{22}	326.5601	360.4257	500.6499	-748.7844	339.1351	291.7178	343.2284	-381.6224	342.2235	254.9154
σ_{33}	586.9049	556.1500	504.5664	315.9052	403.8328	399.1250	398.4050	188.4803	396.1588	315.8979
σ_{iso}	344.7284	382.2437	480.3514	-426.2854	345.7812	308.8644	343.3984	-352.8449	340.1931	273.1023
σ_{aniso}	363.2648	260.8594	36.3226	1113.2858	87.0774	135.3909	82.5099	811.9879	83.9487	64.1933
5AFX										
ppm	P2	O3	P4	O5	O6	O7	O8	O9	N12	N15
σ_{11}	493.0153	347.4844	489.2774	367.7419	355.8661	195.7888	348.2661	348.5479	275.3916	252.7710
σ_{22}	535.3338	352.3542	543.7332	406.9306	384.9345	418.3030	379.6779	382.8813	297.8433	275.4504
σ_{33}	732.1662	405.8583	733.5645	478.7720	452.7585	452.7278	451.8487	459.2721	308.5416	280.4190
σ_{iso}	586.8385	368.5656	588.8584	417.8149	397.8530	355.6065	393.2642	396.9004	293.9255	269.5468
σ_{aniso}	217.9917	55.9390	217.0592	91.4357	82.3582	145.6819	87.8767	93.5575	21.9241	16.3083
4QPF										
ppm	N1	N9	P12	P13	F14	O15	O16	O17	O18	O19
σ_{11}	166.6870	-120.2309	371.2924	358.5225	406.5801	185.5508	276.8187	255.1893	185.6137	248.4056
σ_{22}	186.8310	80.5403	503.9686	498.5045	498.5821	332.2648	341.4780	322.6068	320.2219	337.7732
σ_{33}	291.5409	299.1759	577.4020	574.9991	567.7987	413.9534	417.7479	396.9123	394.3093	420.6935
σ_{iso}	215.0196	86.4951	484.2210	477.3420	490.9870	310.5896	345.3482	324.9028	300.0483	335.6241
σ_{aniso}	114.7819	319.0212	139.7714	146.4856	115.2175	155.0456	108.5995	108.0142	141.3915	127.6041

(*Continued*)

3DYG										
ppm	N3	P9	O10	P11	O12	O13	O14	O15	O16	F18
σ_{11}	272.2813	468.8130	307.8918	494.3100	330.5002	344.9279	175.2842	134.7427	326.4399	252.6723
σ_{22}	285.0418	583.9536	335.7405	574.0939	347.2339	351.1869	441.7081	417.8427	351.6728	454.1963
σ_{33}	304.0441	785.9277	410.4521	740.6575	428.8972	427.1516	497.7941	502.7569	456.0036	627.1797
3DYG										
σ_{iso}	287.1224	612.8981	351.3615	603.0205	368.8771	374.4222	371.5955	351.7808	378.0388	444.6828
σ_{aniso}	25.3825	259.5444	88.6359	206.4555	90.0302	79.0942	189.2979	226.4642	116.9472	273.7454
2F92										
ppm	P2	O3	P4	O5	O6	O7	O8	O9	O10	N14
σ_{11}	129.2678	327.5810	124.9174	285.3878	286.3320	-785.0432	287.4519	293.0829	-819.4334	273.0277
σ_{22}	324.5278	354.8863	341.2007	349.7245	344.7701	-699.3138	340.8483	341.6639	-729.5357	304.4646
σ_{33}	582.9983	397.7685	557.8503	424.7552	409.7726	323.2857	404.3027	404.4552	321.4145	317.5097
σ_{iso}	345.5979	360.0786	341.3228	353.2892	346.9582	-387.0238	344.2010	346.4007	-409.1849	298.3340
σ_{aniso}	356.1005	56.5349	324.7913	107.1991	94.2215	1065.4642	90.1526	87.0818	1095.8991	28.7636
2I19										
ppm	N1	N7	P10	P11	O12	O13	O14	O15	O16	O17
σ_{11}	-110.1587	266.0135	124.5896	317.4599	261.2164	277.3089	-1116.5483	-804.1879	294.1071	293.5133
σ_{22}	74.1505	291.1718	337.2575	380.6968	325.1630	323.4823	-164.9932	-716.7470	346.6974	346.7134
σ_{33}	340.0101	343.8731	583.1254	644.4727	371.1527	367.3362	432.5164	321.0844	410.5222	415.7349
σ_{iso}	101.3340	300.3528	348.3242	447.5432	319.1774	322.7091	-283.0084	-399.9502	350.4423	351.9872
σ_{aniso}	358.0142	65.2805	352.2019	295.3944	77.9630	66.9405	1073.2871	1081.5518	90.1200	95.6216

The computed results have indicated the SCF GIAO Magnetic shielding tensor in ppm for oxygen, nitrogen, fluorine, and phosphorus exploring the active site of 5AEL, 5AFX, 4QPF, 3DYG, 2F92, 2I19 complexes of bisphosphonate agents as the drugs for osteoporosis and similar diseases cure. The calculations have been accomplished based on B3LYP/6-311+G (2d,p) level of theory using Gaussian 09 program software [30] and reported in Table 1.

The agents of 5AEL, 4PF, 2F92, 2I19 have approximately shown the identical behavior for various atoms in the active sites of these compounds through the NMR properties (Figure 2a). The bisphosphonate agents of 3DYG, 5AFX have also the similar fluctuation in the magnetic shielding tensor (Figure 2b).

Moreover, the ^{13}C-NMR measurements on 2F92 and 2I19 bisphosphonate agents have demonstrated the active sites of these compounds exploring the most electronegative atoms for adsorbed onto (5,5) armchair SWCNT which represent the maximal shift in TMS B3LYP/6-311+G(2d,p) (Figure 2 c,d).

The CS tensors are yielded by the quantum chemical calculations in principal axes system to estimate the isotropic chemical-shielding (CSI) and anisotropic chemical-shielding (CSA):

$$\text{CSI (ppm)} = (\sigma_{33} + \sigma_{22} + \sigma_{11})/3 \quad (1)$$

$$\text{CSA (ppm)} = \sigma_{33} - (\sigma_{22} + \sigma_{11})/2 \quad (2)$$

Besides, the Onsager model has influenced on the nuclear magnetic resonance data and chemical shielding of H,C,N,O,F,P atoms in 5AEL, 5AFX, 4QPF, 3DYG, 2F92, 2I19 (Figures 2a, 2b). It has been indicated that oxygen atom in 5AEL, 4PF, 2F92, 2I19 (Figure 2a) and nitrogen atom in 3DYG, 5AFX (Figure 2b) has the most effect on the NMR shielding which direct us toward the active site for adsorption onto (5,5) armchair SWCNT.

(a)

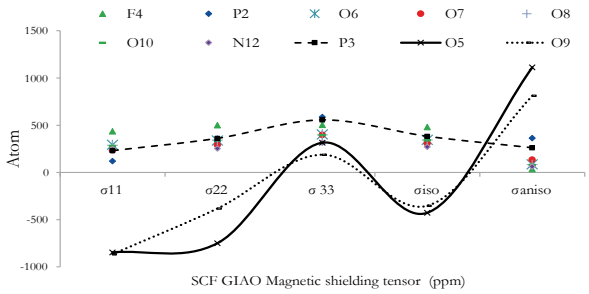

(b)

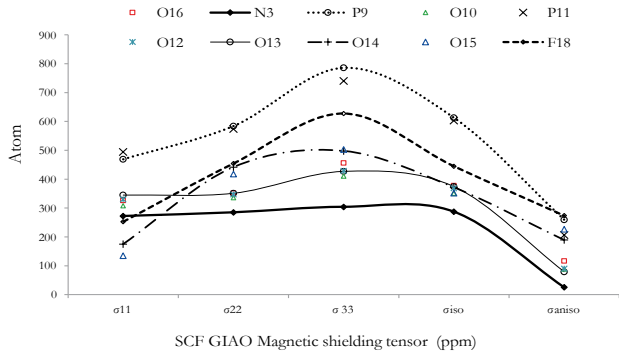

(c)

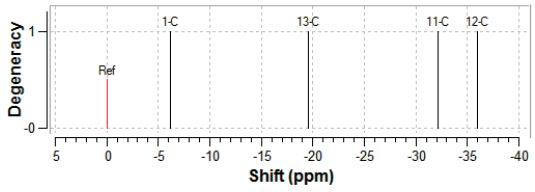

(d)

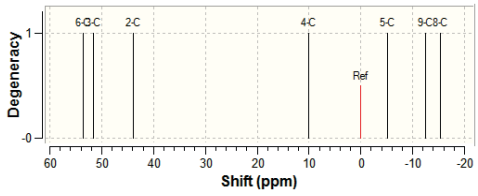

Figure 2. The NMR plot of isotropic (σ_{iso}), anisotropic (σ_{aniso}) and eigenvalue shielding tensors (σ_{11}, σ_{22}, σ_{33}) calculated by level of theory B3LYP/6-311+G(2d,p) for a) 5AEL and similar behavior of 4PF; b) 3DYG and similar behavior for 5AFX in ppm adsorbed site onto (5,5) armchair SWCNT. c) TMS B3LYP/6-311+G(2d,p) for 2F92 , d) TMS B3LYP/6-311+G(2d,p) for 2I19.

IR method

The infrared (IR) calculations have been accomplished for bisphosphonate agents adsorbed onto (5,5) armchair SWCNT using B3LYP method and basis sets of lnl2dz for metal cations of Mg^{2+}, Ca^{2+}, Sr^{2+} and 6-311+G(2d,p) for other atoms including H,C,N,O,F,P to obtain the more accurate equilibrium geometrical parameters, thermodynamic properties and data for each of the determined structure. The IR spectrum for each of two bisphosphonate agents of 2F92 and 2I19 has been seen in the frequency range about 300 cm^{-1} - 4700 cm^{-1} and 1000 - 4600 cm^{-1}, respectively (Figure 3). Figure 3a has shown the strongest allowed peaks about 350, 750, 1100, 4600 cm^{-1} for 2F92 agent and Figure 3b has indicated the highest frequency at 2100, 2750, 3750, 3400 cm^{-1} for 2I19, respectively.

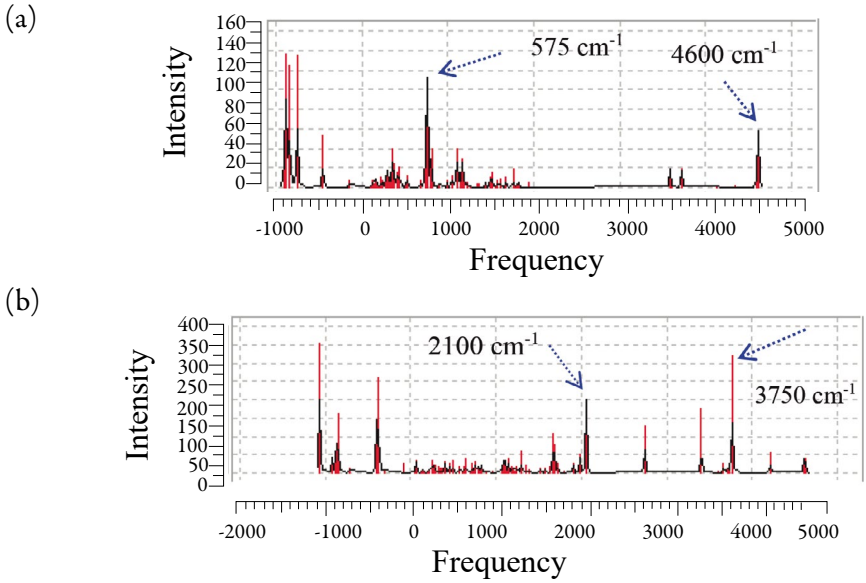

Figure 3. Calculated IR intensity (km/mol) versus frequency (cm^{-1}) through the IR spectra for **a)** 2F92 and **b)** 2I19 of bisphosphonate agents adsorbed onto (5,5) armchair SWCNT using 6-311+G(2d,p) calculations.

The perspective of Figure 3 recommends the reason for existing observed various results of [5AEL, 5AFX, 4QPF, 3DYG, 2F92, 2I19- Mg^{2+}/ Ca^{2+}/Sr^{2+}] complex chelation adsorbed onto (5,5) armchair SWCNT which present the position of active cites of labeled nitrogen, phosphorus, oxygen, fluorine, and metal cations of magnesium, calcium and strontium in these molecules which move the charge of electrons in polar bisphosphonates toward (5,5) armchair carbon nanotube.

Table 2. Calculated functions of harmonic frequencies (cm^{-1}), IR intensities (km/mol) in different normal modes; thermodynamic properties of ΔG, ΔH in kcal/mol and ΔS in cal/mol.K^{-1} at 300 K and optimized energy of UV-Vis.

Compounds	Normal mode	IR Intensity(km/mol)	Frequency(cm^{-1})	$\Delta G \times 10^{-3}$ (kcal/mol)	$\Delta H \times 10^{-3}$ (kcal/mol)	ΔS (cal/K.mol)	$E_{UV\text{-}Vis} \times 10^{-3}$ (kcal/mol)
4QPF	26	24.4465	162.0906	-1045.171	-1045.139	107.498	-111.235
	31	85.3674	356.5734				
	34	332.3113	486.0401				
	35	207.0099	496.4700				
	38	104.2123	595.6733				
	45	150.3644	727.1768				
	66	114.3697	1381.9960				
	69	83.8321	1520.5128				
	76	336.2025	1885.8206				
	79	146.3144	2013.8536				
	82	154.2183	3602.2892				
	90	115.0426	4581.3062				
	92	112.2436	4757.1660				
2F92	33	27.6636	740.9208	-879.212	-879.175	125.093	-86.308
	34	100.7688	761.2168				
	37	38.7864	810.6012				
	41	38.6270	1101.6055				
	42	36.8377	1115.9542				
	44	29.6993	1170.0478				
	58	19.0716	1758.7708				

(*Continued*)

Compounds	Normal mode	IR Intensity(km/mol)	Frequency(cm^{-1})	$\Delta G \times 10^{-3}$ (kcal/mol)	$\Delta H \times 10^{-3}$ (kcal/mol)	ΔS (cal/K.mol)	$E_{UV\text{-}Vis} \times 10^{-3}$ (kcal/mol)
2I19	27	28.6466	399.0835	-936.261	-936.225	119.524	-94.414
	29	34.5129	500.8238				
	33	40.0477	652.4504				
	38	28.0249	789.6133				
	45	32.7104	1084.1391				
	47	31.9705	1110.2915				
	49	38.2129	1142.3353				
	54	57.6366	1302.2768				
	62	106.4028	1673.4444				
	63	75.6871	1681.3981				
	67	49.6146	1986.3383				
	68	200.6094	2058.2918				
	69	126.8656	2742.2821				
	70	173.2174	3408.0867				
	76	320.7285	3765.4924				

Figure3 demonstrates the relationship between intensity and frequency of 2F92 and 2I19 bisphosphonate agents in different normal modes of sharp peaks at B3LYP/6-311+G(2d,p) method. The calculations of the relative harmonic frequencies, IR intensities, and ΔH, ΔG, ΔS for active points of Pyridine and four derivatives of 4QPF, 2F92, 2I19 proteins have been reported in Table2 and plotted in Figures 3 and 4.

It has been notable that polarization functions into the applied basis set in the computations always exist a significant achievement on the simulation and modeling methods of theoretical levels. The normal mode of spectra is exploring of harmonic potential wells by analytic methods which keep the movement of all atoms at the same time in the vibration time scale leading to a natural definition of molecular vibrations (Figure 4).

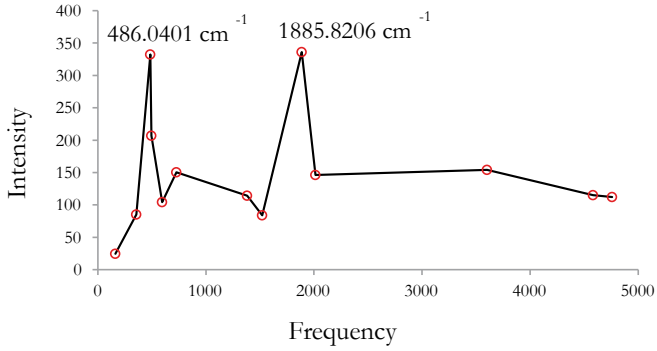

Figure 4. Calculated IR intensity (km/mol) versus frequency (cm^{-1}) for 4QPF bisphosphonate agentadsorbed onto (5,5) armchair SWCNT using 6-311+G(2d,p) calculations.

Therefore, the physico-chemical properties of relative energy (kcal/mol), virial coefficient (-V/T) and dipole moment (Debye) have determined the stability of bisphosphonate agents among [5AEL, 5AFX, 4QPF, 3DYG, 2F92, 2I19- Mg^{2+}/ Ca^{2+}/Sr^{2+}] complex chelation adsorbed onto (5,5) armchair SWCNT as the drugs for preventing the loss of bone cells, cure osteoporosis and other related diseases through the chelated bonding of these compounds with metal cations of Mg^{2+},Ca^{2+} and Sr^{2+} using the drug design method (Table 3 and Figure 5).

The calculated properties describe solubility and permeability for selected bisphosphonates through biological membranes that appear as efficient bioavailability indicators of investigated bisphosphonates, which can be a sufficient methodology to consider in Biopharmaceutical Classification System (BCS) progress.

Table 3. Thermo-physical characteristics of chelated agents of 5AEL, 5AFX, 4QPF, 3DYG, 2F92, 2I19 with metal cations of Mg^{2+}, Ca^{2+} and Sr^{2+} adsorbed onto (5,5) armchair SWCNT at 300 K.

Agent	Metal cation	Relative energy $\times 10^{-4}$ (kcal/mol)	Virial coefficient (-V/T)	Dipole moment (Debye)
5AEL	Mg^{2+}	-96.1388	1.7742	145.3358
	Ca^{2+}	-121.9901	1.7812	1300.1667
	Sr^{2+}	-287.8302	1.9532	1493.9256
5AFX	Mg^{2+}	-95.3258	1.7315	107.7522
	Ca^{2+}	-125.3981	1.7935	2324.3810
	Sr^{2+}	-278.3101	1.9021	2167.8034
4QPF	Mg^{2+}	-111.8961	1.9775	1129.6319
	Ca^{2+}	-143.1309	1.9718	400.0616
	Sr^{2+}	-278.6289	1.9322	996.8129
3DYG	Mg^{2+}	-97.5459	1.8519	842.3853
	Ca^{2+}	-128.6732	1.8940	866.5176
	Sr^{2+}	-292.4445	1.9955	218.6805
2F92	Mg^{2+}	-93.4189	1.9444	597.7910
	Ca^{2+}	-127.7160	1.9794	182.2738
	Sr^{2+}	-277.3898	1.9909	609.9441
2I19	Mg^{2+}	-91.2341	1.8483	601.3917
	Ca^{2+}	-119.3336	1.8754	476.6908
	Sr^{2+}	-285.0652	1.9994	548.9973

Figure 5 has exhibited that the six atoms of oxygen in each site of the bisphosphonate agents chelated to metal cations of Mg^{2+} , Ca^{2+} , Sr^{2+}in 5AEL, 5AFX, 4QPF, 3DYG, 2I19, 2F92 drugs have been minimized by ab-initio method using DFT level which includes ECP calculations with theoretical levels of LANL2DZ for metal elements.

Strontium (Sr) is known for its capability to increase bone and teeth mineralization, osteogenesis, and angiogenesis and downgrading osteoclast activity. This element as one of the main compounds of the bone tissues has a direct impact on metabolism of the bone. For improving bone cure, various investigations have concentrated on the substitution of calcium ions by strontium ions in the structure of bioactive glasses, which can be used for cure of vertebral complex fractures.

The results of the above observations strongly suggest that the different data observed of 5AEL, 5AFX, 4QPF, 3DYG, 2I19, 2F92 in the solvent is predominantly due to basis set functions are induced by a change in polarity of the environment. It is clear that an increase in the dielectric constants increases the stability and efficiency of these bisphosphonate drugs for preventing the loss of bone density and osteoporosis remedy [49-53].

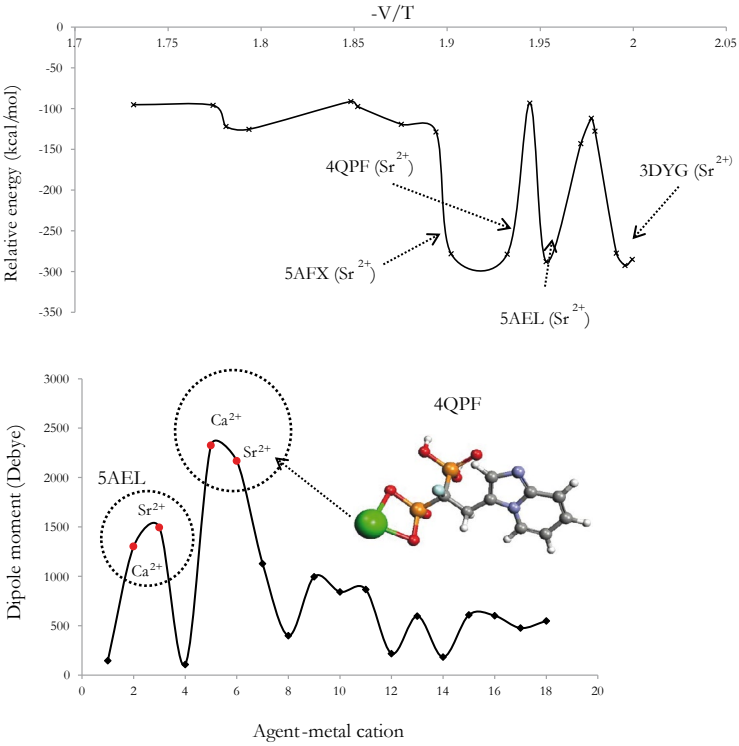

Figure5. a) Relative energy versus Virial coefficient (-V/T) **b)** Dipole moment changes for chelated agents of 5AEL, 5AFX, 4QPF, 3DYG, 2F92, 2I19 with metal cations of Mg^{2+}, Ca^{2+} and Sr^{2+} adsorbed onto (5,5)-SWCNT.

Conclusion

Bisphosphonate agents have attracted much attention for the clinical treatment of some skeletal diseases depicted by enhancing of osteoclast-mediated bone resorption. According to this research, by incorporation of chelated magnesium, calcium and strontium ions to bisphosphonate drugs adsorbed onto (5,5) armchair SWCNT, the network compaction would increase owing the larger atomic radius of strontium atom rather than calcium and magnesium, respectively. For improving bone cure, various investigations have concentrated on the substitution of calcium ions by strontium ions in the structure of bioactive glasses, which can be used for cure of vertebral complex fractures.

Conflict of interest

All authors report that they do not have any conflicts of interest.

References

1. M. Kistler-Fischbacher, B.K. Weeks, B.R. Beck, The effect of exercise intensity on bone in postmenopausal women (part 2): A meta-analysis, *Bone*, **143**, 115697 (2021). Doi: https://doi.org/10.1016/j.bone.2020.115697

2. K.E. Åkesson, F.E.A. McGuigan, Closing the osteoporosis care gap, *Curr. Osteoporos. Rep.*, **19**, 58-65 (2021). Doi: https://doi.org/10.1007/s11914-020-00644-w

3. G. Tiwari, R. Tiwari, B. Sriwastawa, L. Bhati, S. Pandey, P. Pandey, S.K. Bannerjee, Drug delivery systems: An updated review, *Int. J. Pharm. Investig.,* **2**(1), 2–11 (2012). *Doi:* https://doi.org/10.4103/2230-973X.96920

4. J. Li, M. Zeng, H. Shan, C. Tong, Microneedle patches as drug and vaccine delivery platform*, Curr. Med. Chem.,* **24**(22), 2413–2422 (2017). Doi*:* https://doi.org/10.2174/0929867324666170526124053

5. R.K. Tekade (editor), *Basic fundamentals of drug delivery,* Academic Press, 2018.

6. T.M. Allen, Drug delivery systems: Entering the mainstream, *Science,* **303**(5665)*,* 1818–1822 (2004). Doi*:* https://doi.org/10.1126/science.1095833

7. A.P. Singh, A. Biswas, A. Shukla, P. Maiti, Targeted therapy in chronic diseases using nanomaterial-based drug delivery vehicles, *Sig. Transduct. Target. Ther.,* **4**(1)*,* 33 (2019). Doi: https://doi.org/10.1038/s41392-019-0068-3

8. S.M.N. Mohsin, M.Z. Hussein, S.H. Sarijo, S. Fakurazi, P. Arulselvan, Y.H. Taufiq-Yap, Characterisation and cytotoxicity assessment of UV absorbers-intercalated zinc/aluminium-layered double hydroxides on dermal fibroblast cells, *Science of Advanced Materials*, **6**(4), 648–658 (2014). Doi: https://doi.org/10.1166/sam.2014.1752

9. B. Saifullah, M.Z. Hussein, S.H. Hussein-Al-Ali, P. Arulselvan, S. Fakurazi, Antituberculosis nanodelivery system with controlled-release properties based on para-amino salicylate-zinc aluminum-layered double-hydroxide nanocomposites, *Drug Des. Devel. Ther.*, **7**, 1365–1375 (2013). Doi: https://doi.org/10.2147/DDDT.S50665

10. F. Barahuie, M.Z. Hussein, S.H. Hussein-Al-Ali, P. Arulselvan, S. Fakurazi, Z. Zainal, Preparation and controlled-release studies of a protocatechuic acid-magnesium/aluminumlayered double hydroxide nanocomposite, *Int. J. Nanomedicine*, **8**, 1975–1987 (2013). Doi: https://doi.org/10.2147/IJN.S42718

11. A.U. Kura, S.H.H.A. Ali, M.Z. Hussein, S. Fakurazi, P. Arulselvan, Development of a controlled-release anti-parkinsonian nanodelivery system using levodopa as the active agent, *Int. J. Nanomedicine*, **8**, 1103–1110 (2013). Doi: https://doi.org/10.2147/IJN.S39740

12. S.M.N. Mohsin, M.Z. Hussein, S.H. Sarijo, S. Fakurazi, P. Arulselvan, T.Y. Hin, Synthesis of (cinnamate-zinc layered hydroxide) intercalation compound for sunscreen application, *Chem. Cent. J.*, 7(1), 26 (2013). Doi: https://doi.org/10.1186/1752-153X-7-26

13. S.M.N. Mohsin, M.Z. Hussein, S.H. Sarijo, S. Fakurazi, P. Arulselvan, Y.H. Taufiq-Yap, Optimization of UV absorptivity of layered double hydroxide by intercalating organic UV-absorbent molecules, *J. Biomed. Nanotechnol.*, **10**(8), 1490–1500 (2014). Doi: https://doi.org/10.1166/jbn.2014.1854

14. X. Cao, W. Deng, M. Fu, *et al.*, Seventy-two-hour release formulation of the poorly soluble drug silybin based on porous silica nanoparticles: in vitro release kinetics and in vitro/in vivo correlations in beagle dogs, *Eur. J. Pharm. Sci.*, **48**(1-2), 64–71 (2013). Doi: https://doi.org/10.1016/j.ejps.2012.10.012

15. R. Ghaffarian, T. Bhowmick, S. Muro, Transport of nanocarriers across gastrointestinal epithelial cells by a new transcellular route induced by targeting ICAM-1, *J. Control. Release*, **163**(1), 25–33 (2012). Doi: https://doi.org/10.1016/j.jconrel.2012.06.007

16. L. Zhang, H. Xue, Z. Cao, A. Keefe, J. Wang, S. Jiang, Multifunctional and degradable zwitterionic nanogels for targeted delivery, enhanced MR imaging, reduction-sensitive drug release, and renal clearance, *Biomaterials*, **32**(20), 4604–4608 (2011). Doi: https://doi.org/10.1016/j.biomaterials.2011.02.064

17. D.S. Bethune, C.H. Kiang, M.S. de Vries, *et al.*, Cobalt-catalysed growth of carbon nanotubes with single-atomic-layer walls, *Nature*, **363**(6430), 605–607 (1993). Doi: https://doi.org/10.1038/363605a0

18. S. Iijima, T. Ichihashi, Single-shell carbon nanotubes of 1-nm diameter, *Nature*, **363**(6430), 603–605 (1993). Doi: https://doi.org/10.1038/363603a0

19. H. Dai, Carbon nanotubes: opportunities and challenges, *Surface Science*, **500**(1–3), 218–241 (2002). Doi: https://doi.org/10.1016/S0039-6028(01)01558-8

20. T.G. Abi, T. Karmakar, S. Taraphder, Proton affinity of polar amino acid sidechain analogues anchored to the outer wall of single walled carbon nanotubes, *Comput. Theor. Chem.*, **1010**, 53–66 (2013). Doi: https://doi.org/10.1016/j.comptc.2013.02.001

21. W. Feng, P. Ji, Enzymes immobilized on carbon nanotubes, *Biotechnol. Adv.*, **29**(6), 889–895 (2011). Doi: https://doi.org/10.1016/j.biotechadv.2011.07.007

22. Q. Chen, T. Kaneko, R. Hatakeyama, Characterization of pulse-driven gas-liquid interfacial discharge plasmas and application to synthesis of gold nanoparticle-DNA encapsulated carbon nanotubes, *Curr. Appl. Phys.*, **11**(5), S63–S66 (2011). Doi: https://doi.org/10.1016/j.cap.2011.05.022

23. Z. Mbese, B.A. Aderibigbe, Bisphosphonate-based conjugates and derivatives as potential therapeutic agents in osteoporosis, bone cancer and metastatic bone cancer, *Int. J. Mol. Sci.,* **22**, 6869 (2021). Doi: https://doi.org/10.3390/ijms22136869

24. M. Rauner, H. Taipaleenmäki, E. Tsourdi, E.M. Winter, Osteoporosis treatment with anti-sclerostin antibodies-mechanisms of action and clinical application, *J. Clin. Med.,* **10**, 787 (2021). Doi: https://doi.org/10.3390/jcm10040787

25. I. Geiger, C. Kammerlander, C. Höfer, R. Volland, J. Trinemeier, M. Henschelchen, T. Friess, FLS-CARE study group, W. Böcker, L. Sundmacher, Implementation of an integrated care programme to avoid fragility fractures of the hip in older adults in 18 Bavarian hospitals—study protocol for the cluster-randomised controlled fracture liaison service FLS-CARE, *BMC Geriatr.*, **21**, 43 (2021). Doi: https://doi.org/10.1186/s12877-020-01966-1

26. K.N. Hayes, N. He, K.A. Brown, A.M. Cheung, D.N. Juurlink, S.M. Cadarette, Over half of seniors who start oral bisphosphonate therapy are exposed for 3 or more years: Novel rolling window approach and patterns of use, *Osteoporos. Int.*, **32**, 1413-1420 (2021). Doi: https://doi.org/10.1007/s00198-020-05794-2

27. A.S. Sølling, D.H. Christensen, B. Darvalics, T. Harsløf, R.W. Thomsen, B. Langdahl, Fracture rates in patients discontinuing alendronate treatment in real Life: A population-based cohort study, *Osteoporos. Int.*, **32**, 1103–1115 (2021). Doi: https://doi.org/10.1007/s00198-020-05745-x.

28. J.-W. Kim, J. Yee, S.-H. Oh, S.-H. Kim, S.-J. Kim, J.-E. Chung, H.-S. Gwak, Machine learning approaches for predicting bisphosphonate-related osteonecrosis in women with osteoporosis using VEGFA gene polymorphisms, *Journal of Personalized Medicine,* **11**, 541 (2021). Doi: https://doi.org/10.3390/jpm11060541

29. B.L. Langdahl, Overview of treatment approaches to osteoporosis, *Br. J. Pharmacol.*, **178**, 1891–1906 (2021). Doi: https://doi.org/10.1111/bph.15024

30. M.J. Frisch, G.W. Trucks, H.B. Schlegel, G.E. Scuseria, M.A. Robb, J.R. Cheeseman, G. Scalmani, *et al.*, Gaussian, Inc., Wallingford CT., 2009.

31. W. Koch, M.C. Holthausen, *A chemist's guide to density functional theory*, 2nd edition, Wiley-VCH, Weinheim, Germany, 2000. pp. 3-64, 93-104.

32. A.D. Becke, Density-functional thermochemistry. III. The role of exact exchange, *J. Chem. Phys.*, **98**(7), 5648-5652 (1993). Doi: https://doi.org/10.1063/1.464913

33. A.D. Becke, Density-functional exchange-energy approximation with correct asymptotic behavior, *Phys. Rev. A*, **38**(6), 3098-3100 (1988). Doi: https://doi.org/10.1103/PhysRevA.38.3098

34. C. Lee, W. Yang, R.G. Parr, Development of the Colle-Salvetti correlation-energy formula into a functional of the electron density, *Phys. Rev. B*, *Condens. Matter.*, **37**(2), 785-789 (1988). Doi: https://doi.org/10.1103/physrevb.37.785

35. P.J. Stephens, F.J. Devlin, C.F. Chabalowski, M.J. Frisch, *Ab initio* calculation of vibrational absorption and circular dichroism spectra using density functional force fields, *J. Phys. Chem.*, **98**(45), 11623-11627 (1994). Doi: https://doi.org/10.1021/j100096a001

36. C.J. Cramer, D.G. Truhlar, PM3-SM3: A general parameterization for including aqueous solvation effects in the PM3 molecular orbital model, *J. Comput. Chem.*, **13**, 1089-1097 (1992). Doi: https://doi.org/10.1002/jcc.540130907

37. D.A. Liotard, G.D. Hawkins, G.C. Lynch, C.J. Cramer, D.G. Truhlar, Improved methods for semiempirical solvation models, *J. Comput. Chem.*, **16**, 422-440 (1995). Doi: https://doi.org/10.1002/jcc.540160405

38. C.C. Chambers, G.D. Hawkins, C.J. Cramer, D.G. Truhlar, Model for aqueous solvation based on class IV atomic charges and first solvation shell effects,

J. Phys. Chem., **100**(40), 16385-16398 (1996). Doi: https://doi.org/10.1021/jp9610776

39. D.J. Giesen, M.Z. Gu, C.J. Cramer, D.G. Truhlar, A universal organic solvation model,*J. Org. Chem.*, **61**(25), 8720-8721 (1996). Doi: https://doi.org/10.1021/jo9617427

40. L.J. Onsager, Electric moments of molecules in liquids, *J. Am. Chem. Soc.*, **58**, 1486-1493 (1936). Doi: https://doi.org/10.1021/ja01299a050

41. J. Tomasi, Cavity and reaction field: "robust" concepts. Perspective on "Electric moments of molecules in liquids", *Theor. Chem. Acc.*, **103**, 196-199 (2000). Doi: https://doi.org/10.1007/s002149900044

42. J. Park, V.R. Pandya, S.J. Ezekiel, A.M. Berghuis, Phosphonate and bisphosphonate inhibitors of farnesyl pyrophosphate synthases: A structure-guided perspective, *Front. Chem.*, **8**, 612728 (2021). Doi: https://doi.org/10.3389/fchem.2020.612728

43. C. Marocco, G. Zimatore, E. Mocini, R. Fornari, G. Iolascon, M.C. Gallotta, V.M. Bimonte, C. Baldari, A. Lenzi, S. Migliaccio, Efficacy of denosumab therapy following treatment with bisphosphonates in women with osteoporosis: A cohort study, *Int. J. Environ. Res. Public Health,* **18**, 1728 (2021). Doi: https://doi.org/10.3390/ijerph18041728

44. J. Park, V.R. Pandya, S.J. Ezekiel, A.M. Berghuis, Phosphonate and bisphosphonate inhibitors of farnesyl pyrophosphate synthases: A structure-guided perspective, *Front. Chem.*, **8**, 612728 (2021). Doi: https://doi.org/10.3389/fchem.2020.612728

45. E. Adjei-Sowah, Y. Peng, J. Weeks, J.H. Jonason, K.L. de Mesy-Bentley, E. Masters, *et al.*, Development of bisphosphonate-conjugated antibiotics to overcome pharmacodynamic limitations of local therapy: Initial results with carbamate linked sitafloxacin and tedizolid, *Antibiotics,* **10**, 732 (2021). Doi: https://doi.org/10.3390/antibiotics10060732

46. S. Tanaka, Y. Tanaka, RANKL as a therapeutic target of rheumatoid arthritis, *J. Bone Miner. Metab.*, **39**(1), 106–112 (2021). Doi: https://doi.org/10.1007/s00774-020-01159-1

47. M. Vassaki, C. Kotoula, P. Turhanen, D. Choquesillo-Lazarte, K.D. Demadis, Calcium and strontium coordination polymers as controlled delivery systems of

the anti-osteoporosis drug risedronate and the augmenting effect of solubilizers, *Appl. Sci.*, **11**, 11383 (2021). Doi: https://doi.org/10.3390/app112311383

48. L. Rauch, R. Hein, T. Biedermann, K. Eyerich, F. Lauffer, Bisphosphonates for the treatment of calcinosis Cutis-A retrospective single-center study, *Biomedicines,* **9**, 1698 (2021). Doi: https://doi.org/10.3390/biomedicines9111698

49. R.A. Fry, K.D. Kwon, S. Komarneni, J.D. Kubicki, K.T. Mueller, Solid-state NMR and computational chemistry study of mononucleotides adsorbed to alumina, *Langmuir*, **22**(22), 9281-9286 (2006). Doi: https://doi.org/10.1021/la061561s

50. E.M. Sarasia, S. Afsharnezhad, B. Honarparvar, F. Mollaamin, M. Monajjemi, Estrogenic active stilbene derivatives as anti-cancer agents: A DFT and QSAR study, *Phys. Chem. Liq.*, **49**, 561-571 (2011). Doi: https://doi.org/10.1080/00319101003698992

51. B. Ghalandari, M. Monajjemi, F. Mollaamin, Theoretical investigation of carbon nanotube binding to DNA in view of drug delivery, *J. Comput. Theor. Nanosci.*, **8**, 1212-1219 (2011). Doi: https://doi.org/10.1166/jctn.2011.1801

52. M. Monajjemi, N. Farahani, F. Mollaamin, Thermodynamic study of solvent effects on nanostructures: Phosphatidylserine and phosphatidylinositol membranes, *Phys. Chem. Liq.*, **50**, 161-172 (2012).Doi: https://doi.org/10.1080/00319104.2010.527842

53. M. Khaleghian, M. Zahmatkesh, F. Mollaamin, M. Monajjemi, Investigation of solvent effects on armchair single-walled carbon nanotubes: A QM/MD study, *Fuller. Nanotub. Carbon Nanostructures*, **19**, 251-261 (2011). Doi: https://doi.org/10.1080/15363831003721757

How to cite this article

F. Mollaamin, M. Monajjemi, Bone therapy through drug delivery of chelated [bisphosphonate-metal ions] adsorbed on the surface of carbon nanotubes, *Rev. Colomb. Cienc. Quim. Farm.*, **52**(2), 741-765 (2023). https://doi.org/10.15446/rcciquifa.v52n2.110734